



RESEARCH LETTER

10.1029/2025GL118361

Key Points:

- Microfluidic visualizations reveal CO₂ hydrate formation and growth in unsaturated porous media
- In unsaturated media, hydrate crystals preferentially grow in narrower paths and accelerate toward the local water pockets
- Explosive crystallization emerges when a growing crystal contacts a water pocket, enabling long-range hydrate propagation

Supporting Information:

Supporting Information may be found in the online version of this article.

Correspondence to:

L. Jiang, K. Xu and Y. Song, lanlan@dlut.edu.cn; kexu1989@pku.edu.cn; songyc@dlut.edu.cn

Citation:

Liu, Q., Hassanpouryouzband, A., Du, Y., Jiang, L., Xu, K., Lv, W., & Song, Y. (2025). Reactive crystallization in unsaturated porous media. *Geophysical Research Letters*, 52, e2025GL118361. https://doi.org/10.1029/2025GL118361

Received 24 JUL 2025 Accepted 26 OCT 2025

Author Contributions:

Conceptualization: Qingbin Liu, Aliakbar Hassanpouryouzband, Yilin Du, Lanlan Jiang, Ke Xu, Yongchen Song Data curation: Qingbin Liu, Aliakbar Hassanpouryouzband, Yilin Du, Weifeng Lv

Funding acquisition: Qingbin Liu, Yilin Du, Lanlan Jiang, Ke Xu, Yongchen Song

Investigation: Qingbin Liu, Aliakbar Hassanpouryouzband, Yilin Du, Weifeng Lv

Methodology: Qingbin Liu, Aliakbar Hassanpouryouzband, Yilin Du, Lanlan Jiang, Ke Xu, Yongchen Song

© 2025 The Author(s).

This is an open access article under the terms of the Creative Commons

Attribution-NonCommercial License, which permits use, distribution and reproduction in any medium, provided the original work is properly cited and is not used for commercial purposes.

Reactive Crystallization in Unsaturated Porous Media

Qingbin Liu¹, Aliakbar Hassanpouryouzband², Yilin Du¹, Lanlan Jiang¹, Ke Xu³, Weifeng Lv⁴, and Yongchen Song¹

¹Key Laboratory of Ocean Energy Utilization and Energy Conservation of the Ministry of Education, School of Energy and Power Engineering, Dalian University of Technology, Dalian, China, ²School of Geosciences, University of Edinburgh, Grant Institute, Edinburgh, UK, ³Department of Energy and Resources Engineering, College of Engineering, Peking University, Beijing, China, ⁴State Key Laboratory of Enhanced Oil & Gas Recovery, Beijing, China

Abstract Crystal nucleation and growth reshape the mechanical, transport and reactive properties in subsurface porous media. We visualize CO₂ hydrate formation and growth in a microfluidic unsaturated porous medium and uncover novel multiscale dynamics: (a) hydrate crystals preferentially grow in narrower paths and seal low-permeability regions, despite lower surface energy in wider pathways; (b) explosive crystallization emerges at water-gas interface when growing crystals touch water pockets, that enables efficient hydrate propagation across disconnected water clusters. These observations are theoretically rationalized. We therefore provide an interpretation of field observations of early stage hydrate enrichment in low permeability zones, and discover a new nucleation propagation mechanism. The mechanism may also emerge in other reactive crystallization in unsaturated media.

Plain Language Summary In efforts to securely store CO₂ underground, one promising method is to trap it as solid hydrates. However, how these hydrates actually grow and reshape flow pathways deep underground remains poorly understood. We observe CO₂ hydrates formation and growth inside an unsaturated microfluidic porous medium, and reveal the microscopic diffusion-driven dynamics. Accordingly, we rationalize field observation that hydrate preferential growth in low-permeability formations, and discover a novel mechanism of nucleation spreading over pores.

1. Introduction

Crystals nucleation and growth commonly emerge in subsurface media, as results of changes in ambient composition, temperature, pressure, or chemical reaction (De Yoreo et al., 2015; Dobberschütz et al., 2018; Godinho et al., 2016; Ma et al., 2023; Righter & Downs, 2001). Examples include permafrost freezing (Creel et al., 2024; Ma et al., 2023; Righter & Downs, 2001), CO₂ sequestration as carbonate minerals in deep stratum (Boot-Handford et al., 2014; Cao et al., 2007; DePaolo & Cole, 2013; Guida et al., 2017; Seyyedi et al., 2020), salt precipitates in groundwater (Clarke et al., 2022; Ji et al., 2025; Shokri-Kuehni et al., 2017) or after engineering gas storage (Braid et al., 2024; Falcon-Suarez et al., 2020; He et al., 2019; Sokama-Neuyam et al., 2023; Yan et al., 2025), deposition of bitumen molecules during oil recovery (Abedini et al., 2011; Doryani et al., 2018; Schultz et al., 2023), and gas hydrates formation (Chong et al., 2016; Liu et al., 2025; Pecher et al., 2025). Crystallization modulates the porous morphology, that alters permeability (Beckingham, 2017; Chen et al., 2024; Nooraiepour et al., 2018), distorts flow and transport paths (Chagneau et al., 2015), generates internal stresses (Scherer, 2000), or even induces microcracks that destabilize the stratum (Espinosa-Marzal & Scherer, 2010).

In porous media, crystallization from multiphase/fluid is governed by the dynamics at fluid-fluid/solid interfaces by which spatially segregate reactive components. For example, gas hydrate formation in subsurface is at the interface of gas and water (Gu et al., 2025; Sloan, 2003; Xu et al., 2024); salt precipitation in flow-through drying is highly regulated by the dynamic brine-gas interface evolution (Li et al., 2024); additionally, in mineralization trapping for CO_2 sequestration, CO_2 dissolves in formation water and interacts with the rock (Seyyedi et al., 2020). While crystallization in a single, homogeneous phase can be described by classical Lifshitz-Slyozov-Wagner (LSW) theory, the anisotropic and heterogeneous distribution of phases in unsaturated porous media defies such uniform assumptions (Budke et al., 2009; Svoboda et al., 2022). There is still no consensus on the morphology and kinetics of crystallization in unsaturated porous media within multiphase fluid systems.

In this study, we visualize the growth of CO₂ hydrate crystals within a microfluidic porous medium. We first perform continuous CO₂ injection into a water-saturated porous medium until achieving irreducible water

LIU ET AL.



10.1029/2025GL118361

Project administration: Ke Xu,
Yongchen Song
Supervision: Qingbin Liu,
Aliakbar Hassanpouryouzband, Yilin Du,
Lanlan Jiang, Ke Xu, Weifeng Lv,
Yongchen Song
Validation: Qingbin Liu,
Aliakbar Hassanpouryouzband
Visualization: Qingbin Liu,
Aliakbar Hassanpouryouzband
Writing – original draft: Qingbin Liu,
Aliakbar Hassanpouryouzband
Writing – review & editing: Qingbin Liu,
Aliakbar Hassanpouryouzband, Yilin Du,
Lanlan Jiang, Ke Xu

saturation, and then maintain system closure with constant gas pressure at 3.5 MPa. We capture the nucleation, growth and ripening of hydrates in situ and visualize local crystallization kinetics and crystals' spatial distribution evolution in unsaturated media. We expect to provide a benchmark for future multi-scale modeling studies on subsurface geochemical and reactive transport processes.

2. Materials and Methods

2.1. Materials

Carbon dioxide (Dalian Special Gases Co., Ltd., China, with a purity of 99%) is used as the gas source. Nitrogen (Dalian Special Gases Co., Ltd., China, with a purity of 99%) is used for confining pressure. Deionized water is used in the hydrate formation processes. Calcium chloride (Shanghai Macklin Biochemical Technology Co., Ltd., China) is used to prepare salt water.

2.2. Methods

Observations of hydrate phase transitions are performed in a microfluidic system (Figure S1 in Supporting Information S1). The microfluidic chip is custom-designed and fabricated based on micro-CT scans of actual rock cores. After acquisition, the slice images are refined and converted into the chip layout, which is then etched 50 µm deep. The microfluidic chip is placed in a high-pressure chamber for high-pressure operations. The experimental setup includes fluid injection module, temperature and pressure control module, and data acquisition module. Fluid injection is performed using an ISCO pump (260D, Teledyne Isco Inc., Lincoln, NE, USA) and a high-precision syringe pump (LC-3060, Chin-Fine Technology). The entire experimental system is temperature-controlled using a thermostatic bath (300F, JULABO), while pressure is maintained by the ISCO pump in conjunction with a back-pressure valve. A CCD camera (QSI6120WS, ATIK), coupled with a microscope (12X Zoom, NAVITAR), is used to real-time record the hydrate growth behavior inside the microfluidic chip. Pressure sensors are installed at the inlet and outlet of the microfluidic chip to monitor the pressure at both ends of the chip. The contact angle of the etched pores is measured at 32.17°, confirming their hydrophilic nature (Figure S1e in Supporting Information S1).

The main experimental procedures can be summarized as follows. First connect the piping and check for leaks, then evacuate the entire system for 1h to eliminate interference from remaining gases. Nitrogen gas with a stable pressure of 4.0 MPa is injected into the confining pressure device, to ensure that the confining pressure is higher than the experimental pressure. The system temperature is set at 275.15 K. The backpressure is set at 3.5 MPa, while the micromodel is gradually saturated with water and pressurizes to the same level. Maintain the back pressure of 3.5 MPa. Carbon dioxide gas with an initial pressure of 3.6 MPa is injected into the micromodel to displace part of the water. After that, set the pressure to 3.5 MPa. And then, waiting for the hydrate to form.

3. Results and Discussion

3.1. Overview of Hydrate Crystal Nucleation and Growth

Prior to crystallization, water occupies 32.8 vol % of the pore space, residing predominantly in concave "corner" and dead end pores in accordance with the well-established preference of wetting fluids for high-specific area regions (Gao et al., 2022; Helland & Jettestuen, 2016; Moebius & Or, 2014; Stocker & Hosoi, 2004; Wu et al., 2018; Yang et al., 2013), as shown in Figure 1a. During crystal formation and growth, the residual water pockets correspondingly shrink as compensation (Figure 1b and Figure S2 in Supporting Information S1). Water saturation decreases dramatically from 32.8% to 27.0% within 12 min, and then decreases by 13.5% in the following 48 hr, corresponding to rapid nucleation and slow growth of hydrates.

In individual pores and channels, hydrate evolution conforms to classical nucleation theory: nuclei appear stochastically along gas-water interfaces of some water pockets, forming a thin film that can enclose an entire water pocket within 1 min (Figure 1a). Subsequently, growth proceeds concurrently into both gas and liquid phases (Text S1 in Supporting Information S1), with discrete crystals extending into the gas and clustered aggregates developing in the liquid. As expected, in the gas phase, local coarsening causes some nuclei to vanish while others continue growing until a single crystal outcompetes its neighbors. Crystals growing into gas phase results in major modification of pore space and gas flow path, which would be the focus of this work.

LIU ET AL. 2 of 10

19448007, 2025, 21, Downloaded from https://agupubs.onlinelibrary.wiley.com/doi/10.1029/2025GL118361 by CochraneChina, Wiley Online Library on [05/11/2025]. See the Terms and Conditions

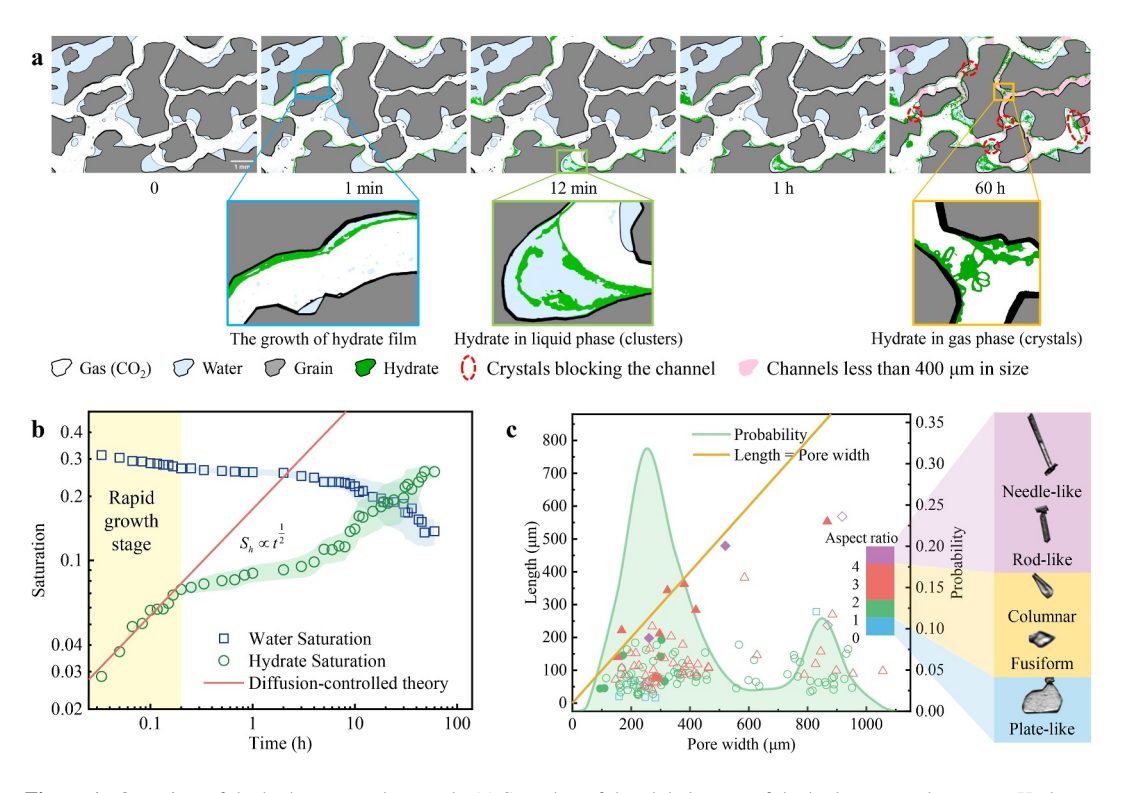


Figure 1. Overview of the hydrate crystals growth. (a) Snapshot of the global status of the hydrate growth process. Hydrate crystals in the dashed red circle block the channel. (b) Water saturation and hydrate saturation over time. S_h represents hydrate saturation. (c) Crystal length distribution for different pore widths at 60th h. Crystal aspect ratio is represented as dots of different shapes with different colors. Solid dots represent crystals occupying the entire pore channel. Points below the yellow line indicate crystal lengths shorter than the channel width. The excess of crystal length over the pore width is likely a result of inclined growth within the confinement.

Globally, hydrate crystals are more aggregated in narrow channels, with over 65.6% of crystals forming in pore throats narrower than $400~\mu m$ (Figure 1c), even though these channels constitute only 24.3% of the pore volume. This striking preference contrasts with classical bubble ripening in porous media, where bubbles in small pores are consumed to feed bubbles' growth in larger pores, which reduces total surface free energy (Mehmani & Xu, 2022a, 2022b).

3.2. Local Inter-Seeds Competition

Numerous micro-crystals form at the very beginning, and competitive interplay among crystals and water pockets are observed. Two representative and synchronized hydrate growth patterns at pore interfaces are shown in Figure 2.

Figure 2a shows typical competitive growth in a micro-channel with average pore width exceeding 400 μ m and initial liquid cluster spanning $4.8 \times 10^4 \ \mu\text{m}^2$. Crystal growth occurs in 3 phases: (a) in the first 8 hr, multiple crystals co-develop slowly, and 3 major crystals survive with the growing facet of crystal #1 right toward the nearby water pocket; (b) after 8 hr, growth of crystal #1 dominates, and quickly accelerates until the crystal touches the water pocket, while crystal #2 and crystal #3 keep slowly growing (Figure 2b); (c) when crystal #1 touches the water pocket, explosive crystallization emerges on water pocket surface, and growth of crystal #2 and crystal #3 is terminated.

Figure 2c shows another typical synchronized growth of multiple dominant crystals within a narrow long channel with two water pockets along a concave boundary. After 2 hr, crystal #4, crystal #5 and crystal #6 that nucleate on the same side of the channel survive. In the following competition, crystal #5, which sits at the narrowest throat along the channel, dominates over its neighbors and grow toward the other side with water pocket (Red box in Figure 2d), where the presence of a liquid film can be identified (Figure S3 in Supporting Information S1). When crystal #5 grows close or even touches the solid wall, the growth rate reduces as the high-energy facet does not

LIU ET AL. 3 of 10

19448007, 2025, 21, Downloaded from https://agupubs.onlinelibrary.wiley.com/doi/10.1029/2025GL118361 by CochraneChina, Wiley Online Library on [05/11/2025]. See the Terms

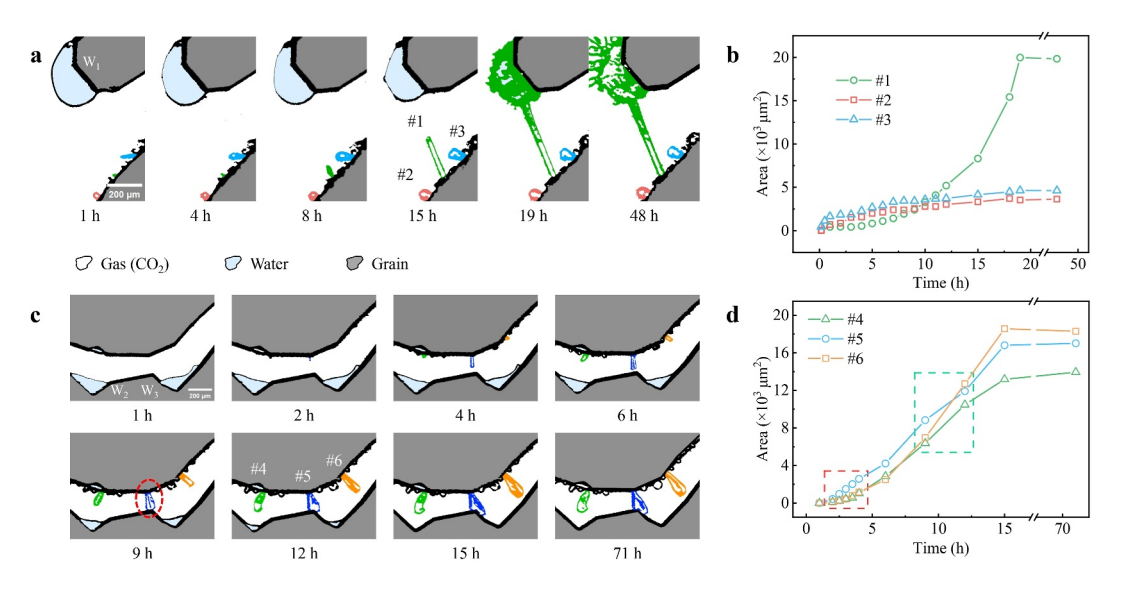


Figure 2. Simultaneous growth of multiple crystals in the pore. (a, c) Snapshots of multiple hydrate crystals growth. (b) Quantification of crystal area in panel (a). The line color corresponds to the crystal color separately. (d) Quantification of crystal area in panel (c). The line color corresponds to the crystal color separately.

expose to the vapor anymore, and neighboring crystals (crystal #4 and crystal #6) are allowed to re-start growth (Green box in Figure 2d). By this time, crystal #5 has effectively blocked the throat.

3.3. Water Vapor Transport Regulates Single Crystal Growth

Although the global growth rate of hydrates decelerates, growth of a local dominant crystal accelerates in presence of local water pocket. To illustrate this behavior, we track the area evolution of four representative crystals situated in distinct pore geometries (Figure 3a). With sufficient water, all crystals exhibit progressive acceleration (Figure 3b). Growth is terminated when the water source disappears (water depletion for crystal #7 and water-to-hydrate conversion for crystal #8), or when the growing facet of the crystal contacts the water pocket and induces further explosive nucleation on its surface (crystal #9 and crystal #10).

The formation and accelerating growth of crystals toward local water pocket imply that hydrate formation in porous media is directed by residual water, and limited by mass transfer of water vapor through gas phase from residual water pocket. As high energy crystal facets consume nearby vapor, they create a local pressure minimum that induces a vapor pressure gradient and sustains vapor flux from adjacent water pockets. Growth of a typical crystal can be divided into two stages:

- 1. Formation of local dominant crystal. At the very beginning, many nucleates emerge with different distance to water pocket and different facing directions of growing facet. On one hand, nucleates closer to the water pocket have lower diffusion distance for water and thus get more sufficient water vapor supply; on the other hand, nucleates with growing facet (high-energy facet) directing to the water pocket can reduce water vapor transfer distance faster than its neighbors. As a result, a crystal that have smallest distance to water pocket and growing direction right toward the water pocket finally dominates, as shown in abovementioned examples.
- Accelerating dominant crystal growth. Once a dominant crystal is selected, its further growth would reduce the
 distance between the growing facet and the water pocket, that results in an accelerating growth rate (Mullin, 2001; Sloan, 1998; Titze et al., 2015; Figure 3c). Assuming that only the high-energy facet grows, the
 kinetics should follow:

$$\frac{dA}{dt} \propto \frac{1}{x} \tag{1}$$

where A denotes the area of the crystal and x denotes the distance between the crystal front and the target water source. This correlation is well-supported by experimental measurements (Figure 3d). Equation 1 describes the

LIU ET AL. 4 of 10

19448007, 2025, 21, Downloaded from https://agupubs.onlinelibrary.wiley.com/doi/10.1029/2025GL118361 by CochraneChina, Wiley Online Library on [05/11/2025]. See the Terms and Con

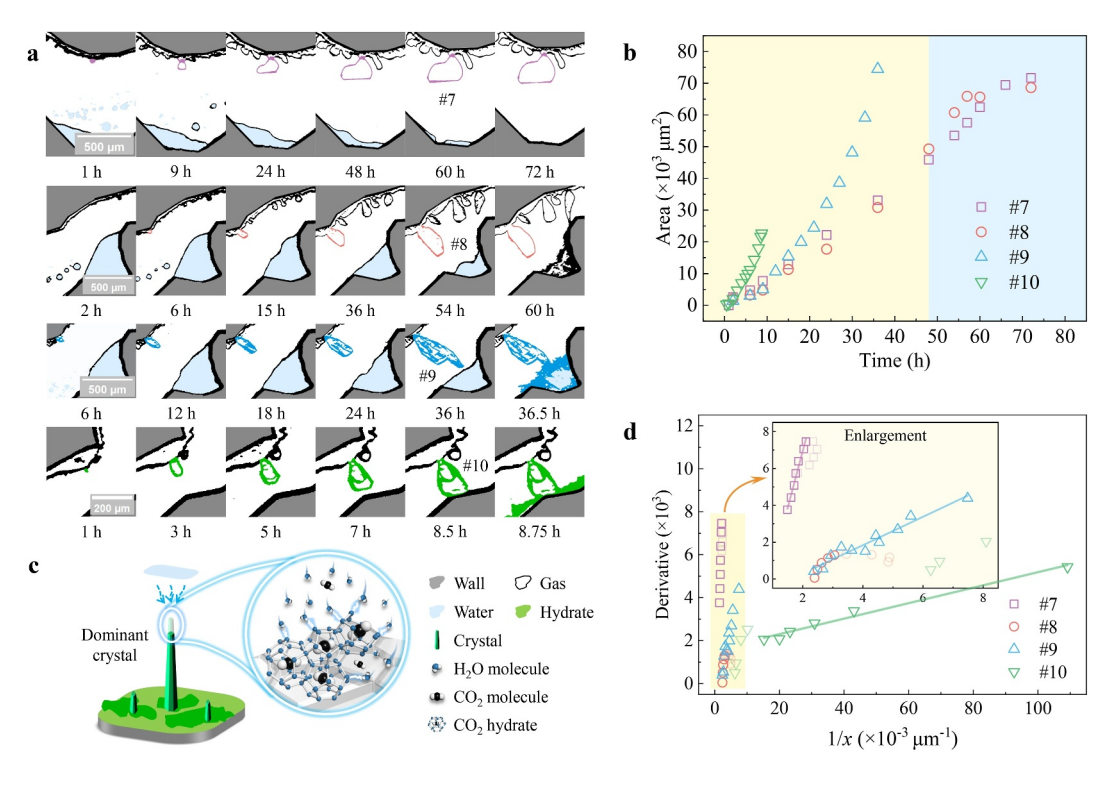


Figure 3. Study on the growth rate of hydrate crystals. (a) Snapshot of hydrate crystal growth. (b) Variation of crystal area with time. (c) Diagram of the mechanism of crystal growth. (d) Relationship between the derivative of the crystal area curve and 1/x.

approximate relationship within the intermediate x interval. However, this model becomes inapplicable as x approaches 0, where saturation effects must be accounted for. This limitation arises from the transition in the rate-limiting step of crystal growth, which is generally governed by mass transfer but shifts to the crystallization reaction when the crystal is sufficiently close to the water source. In this regime, the interfacial reaction rate becomes the rate-limiting step, and further reduction in x does not significantly enhance the growth rate. Under these conditions, the reaction kinetics are expected to follow:

$$\frac{dA}{dt} \propto \frac{1}{a+x} \tag{2}$$

where a is a constant associated with the crystallization reaction process, likely related to the thickness of the reaction boundary layer. However, our experimental sampling resolution precludes a definitive determination of a, as we lack data in the requisite small-x interval. Since this reaction-dominated regime is not the primary focus of our work, we do not explore it further.

Complementary ice crystal growth experiments (Text S2 in Supporting Information S1) reveal similar behavior, underscoring the broad applicability of these kinetic mechanisms. This accelerating crystal growth is also supported by Raman spectroscopic experiments (Ou et al., 2016).

3.4. Preferential Crystal Growth in Narrow Channels

It is well accepted that discrete phases in porous media prefer to emerge in larger pores or wider channels, to minimize surface energy (Emmanuel et al., 2010; Poonoosamy et al., 2023). However, our experimental observation shown in Figure 1c does not match it, as 65.6% of the crystals are distributed in narrow channels.

The preceding analysis of individual and collective crystal growth reveals that vapor limited kinetics govern hydrate distribution: narrow channels not only offer higher specific surface areas for nucleation but also impose shorter vapor diffusion paths, accelerating local water vapor transport. In addition, due to the presence of water

LIU ET AL. 5 of 10

19448007, 2025, 21, Downloaded from https://agupubs.onlinelibrary.wiley.com/doi/10.1029/2025GL118361 by CochraneChina

Figure 4. Difference in phase distribution between wide and narrow channels. (a) Diagram of the mechanism of liquid self-flow effect. (b) Variation of crystal saturation with time. Crystal saturation refers to the volume fraction of pore space occupied by crystals in the channel.

film and corner flow in hydrophilic porous media (Figure 4a), water can dynamically redistribute between wider and narrower channels, that further secures the water supply in narrow channel (Lebeau & Konrad, 2010; Tokunaga, 2009; Wu et al., 2020).

As a result, crystal growth concentrates within low-permeability paths (Figure 4b), further constricting narrow paths while leaving wider paths largely unaltered. This selective pore clogging remodels the pore space, and may modify the stress chain (Li et al., 2023; Liu et al., 2020; Zhang et al., 2020), that result in major transport and mechanical consequences at larger scales.

Nevertheless, as wider channels have a lower minimum free energy, we do not exclude the possibility that hydrate would slowly ripen and re-concentrate into wider paths, over geological time scale. This observation echoes field observation that hydrates always form in low-permeability region and migrates afterward (Bagherzadeh et al., 2011; Bai et al., 2024; Ge et al., 2019), although classic rationalization emphasizes the enrichment of carbon source in low-permeability region.

3.5. Explosive Nucleation and Inter-Pocket Nucleation Propagation

With sufficient water supply, a dominant crystal penetrates the gas phase and touches the water pocket. It surprisingly induces explosive nucleation at the gas-water interface, that further evolves into hydrate cluster covering the whole water pocket surface (Figure 5a). Remarkably, this contact-induced hydrate-covering occurs within 1 min, that is much faster than diffusion-driven crystal growth discussed above.

We attribute this explosive nucleation after merging of high-energy crystal facet into water pocket to a few synergistic mechanisms:

- 1. Jump-up of water vapor pressure. When the high-energy face is still exposed to the gas phase, it behaves as a water vapor sink and generates a local minimum of water vapor pressure that is below the critical pressure for nucleation. However, when the crystal surface contacts fluid-fluid interface, the surrounding vapor pressure accordingly jumps up, that may allow crystallization in nearby region.
- 2. Formation of heterogeneous crystallization site. The crystal-water-gas contact line acts as a heterogeneous catalytic site (Figure 5b), reducing the free energy barrier for nucleation and thereby initiate crystallization covering the water-gas surface (Baek et al., 2020; Bai et al., 2015; Fornea et al., 2009; Shaw et al., 2005; Sun & Tanaka, 2024).
- 3. Local enrichment of CO₂ before contacting. To maintain pressure equilibrium during the slow process, local unsaturated water vapor pressure near the growing face of the crystal results in local enrichment of CO₂. Therefore, when the crystal tip is close to the water pocket surface, it results in higher solubility of CO₂ in the water pocket, which is then released after crystal-water contact and contribute to nucleation.

We note that this explosive nucleation does not only have local consequences. It allows crystal formation to propagate among topologically discrete residual liquid pockets. It therefore provides an efficient route to spread

LIU ET AL. 6 of 10

19448007, 2025, 21, Downloaded from https://agupubs.onlinelibrary.wiley.com/doi/10.1029/2025GL118361 by CochraneChina, Wiley Online Library on [05/11/2025]. See the Terms

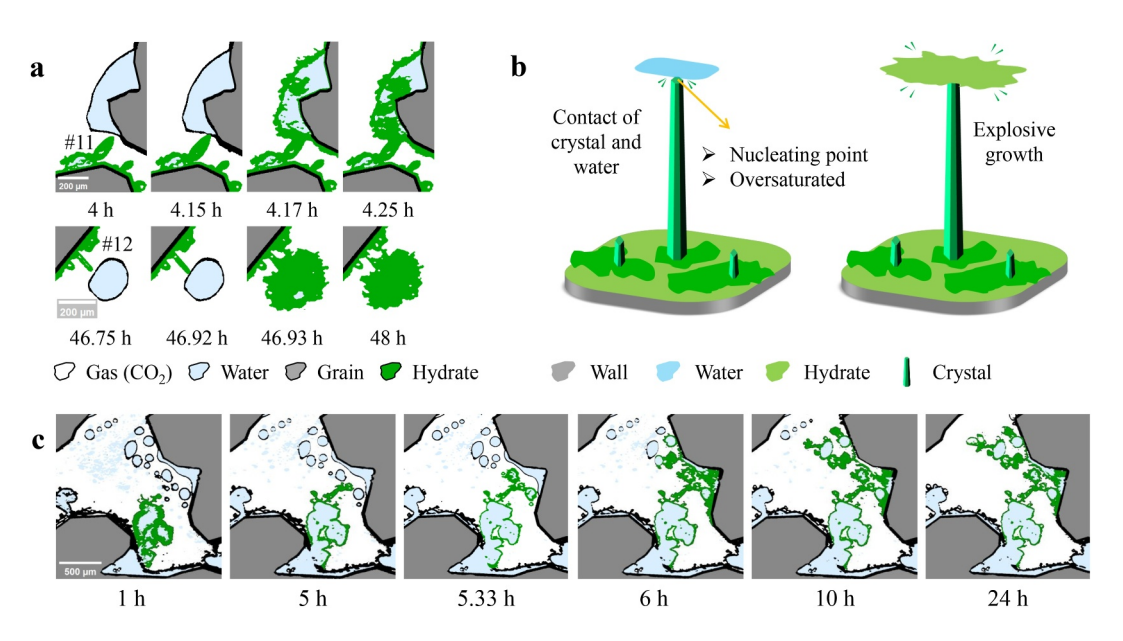


Figure 5. Contact of crystals with water and induced-nucleation of the water source. (a) Snapshots of rapid nucleation due to crystal contact with water. (b) Diagram of the mechanism of crystal-induced nucleation and hydrate cluster explosive growth. (c) Continuous nucleation of discontinuous gas-water interface induced by growing crystals.

local crystallization over long distance, breaking through the limitation of water phase poor connectivity (Figure 5c). Growth or movement of crystals in the liquid phase can lead to similar hydrate propagation (Zhang et al., 2024).

4. Conclusions

In this study, we adopt CO₂ hydrates as a model system to visualize crystal growth in unsaturated porous media. We uncover two unique behaviors and rationalize them with experimental and theoretical evidences:

- 1. Preferential formation of crystals in narrow channels and directional growth of local dominate crystal acceleratingly toward a nearby water pocket, that efficiently block the low-permeability region and reshape the pore space morphology and stress chain.
- 2. Explosive nucleation that rapidly covers the water pocket surface, which provides a route for nucleation propagation over long distance among discrete residual water pockets.

These discoveries advance the fundamental understanding of hydrate nucleation and growth in confined environments, with wide-ranging engineering implications. In the context of CO_2 sequestration, our findings offer insights into the hydrate-based trapping method by elucidating how hydrate growth patterns evolve within pore networks. This knowledge can aid in predicting and controlling the location, growth rate, and long-term stability of CO_2 hydrate deposits. These findings are also relevant to natural gas hydrate production by improving predictions of hydrate distribution, saturation, and growth behavior. The revealed mechanisms can be generated into broader cases of crystallization in unsaturated media, where key components for crystal formation mainly distribute in distinct phases.

Conflict of Interest

The authors declare no conflicts of interest relevant to this study.

Data Availability Statement

Data used in this study is available at Zenodo (Liu, 2025).

LIU ET AL. 7 of 10



10.1029/2025GL118361

Acknowledgments

This work was supported by the National Natural Science Foundation of China (Grant 52176057, U23B6004 [Joint Fund], 52020105007), and the National Science and Technology Major Project in China (Grant 2024ZD1406602).

References

- Abedini, A., Ashoori, S., & Torabi, F. (2011). Reversibility of asphaltene precipitation in porous and non-porous media. *Fluid Phase Equilibria*, 308(1–2), 129–134. https://doi.org/10.1016/j.fluid.2011.06.024
- Back, S., Lee, W., Min, J., Ahn, Y. H., Kang, D. W., & Lee, J. W. (2020). Hydrate seeding effect on the metastability of CH₄ hydrate. *Korean Journal of Chemical Engineering*, 37(2), 341–349. https://doi.org/10.1007/s11814-019-0451-3
- Bagherzadeh, S. A., Moudrakovski, I. L., Ripmeester, J. A., & Englezos, P. (2011). Magnetic resonance imaging of gas hydrate formation in a bed of silica sand particles. *Energy and Fuels*, 25(7), 3083–3092. https://doi.org/10.1021/ef200399a
- Bai, C., Wang, H., Li, Q., Zhang, Y., & Xu, X. (2024). Controls on deep and shallow gas hydrate reservoirs in the Dongsha Area, South China Sea: Evidence from sediment properties. *Journal of Marine Science and Engineering*, 12(5), 696. https://doi.org/10.3390/jmse12050696
- Bai, D., Chen, G., Zhang, X., Sum, A. K., & Wang, W. (2015). How properties of solid surfaces modulate the nucleation of gas hydrate. *Scientific Reports*, 5, 1–12. https://doi.org/10.1038/srep12747
- Beckingham, L. E. (2017). Evaluation of macroscopic porosity-permeability relationships in heterogeneous mineral dissolution and precipitation scenarios. Water Resources Research, 53(12), 10217–10230. https://doi.org/10.1002/2017WR021306
- Boot-Handford, M. E., Abanades, J. C., Anthony, E. J., Blunt, M. J., Brandani, S., Mac Dowell, N., et al. (2014). Carbon capture and storage update. *Energy & Environmental Science*, 7(1), 130–189. https://doi.org/10.1039/c3ee42350f
- Braid, H., Taylor, K., Hough, E., Rochelle, C., Niasar, V., & Ma, L. (2024). Hydrogen-induced mineral alteration: A review in the context of Underground Hydrogen Storage (UHS) in saline aquifers. *Earth-Science Reviews*, 259, 104975. https://doi.org/10.1016/j.earscirev.2024.
- Budke, C., Heggemann, C., Koch, M., Sewald, N., & Koop, T. (2009). Ice recrystallization kinetics in the presence of synthetic antifreeze glycoprotein analogues using the framework of LSW theory. *Journal of Physical Chemistry B*, 113(9), 2865–2873. https://doi.org/10.1021/ip057366
- Geophysical Research Letters, 34(5), https://doi.org/10.1029/2006GL028605
- Chagneau, A., Claret, F., Enzmann, F., Kersten, M., Heck, S., Madé, B., & Schäfer, T. (2015). Mineral precipitation-induced porosity reduction and its effect on transport parameters in diffusion-controlled porous media. *Geochemical Transactions*, 16(1), 1–16. https://doi.org/10.1186/s12932-015-0027-z
- Chen, X. S., Hu, R., Zhou, C. X., Xiao, Y., Yang, Z., & Chen, Y. F. (2024). Capillary-Driven backflow during salt precipitation in a rough fracture. Water Resources Research, 60(3), 1–20. https://doi.org/10.1029/2023WR035451
- Chong, Z. R., Yang, S. H. B., Babu, P., Linga, P., & Li, X. S. (2016). Review of natural gas hydrates as an energy resource: Prospects and challenges. *Applied Energy*, 162, 1633–1652. https://doi.org/10.1016/j.apenergy.2014.12.061
- Clarke, C. E., Vermooten, M., Watson, A., Hattingh, M., Miller, J. A., & Francis, M. L. (2022). Downward migration of salts in termite-affected soils: Implications for groundwater salinization. *Geoderma*, 413(September 2021), 115747. https://doi.org/10.1016/j.geoderma.2022.115747
- Creel, R. C., Miesner, F., Wilkenskjeld, S., Austermann, J., & Overduin, P. P. (2024). Glacial isostatic adjustment reduces past and future Arctic subsea permafrost. *Nature Communications*, 15(1), 3232. https://doi.org/10.1038/s41467-024-45906-8
- DePaolo, D. J., & Cole, D. R. (2013). Geochemistry of geologic carbon sequestration: An overview. *Reviews in Mineralogy and Geochemistry*, 77(1), 1–14. https://doi.org/10.2138/rmg.2013.77.1
- De Yoreo, J. J., Gilbert, P. U. P. A., Sommerdijk, N. A. J. M., Penn, R. L., Whitelam, S., Joester, D., et al. (2015). Crystallization by particle attachment in synthetic, biogenic, and geologic environments. *Science*, 349(6247), aaa6760. https://doi.org/10.1126/science.aaa6760
- Dobberschütz, S., Nielsen, M. R., Sand, K. K., Civioc, R., Bovet, N., Stipp, S. L. S., & Andersson, M. P. (2018). The mechanisms of crystal growth inhibition by organic and inorganic inhibitors. *Nature Communications*, 9(1), 1–6. https://doi.org/10.1038/s41467-018-04022-0
- Doryani, H., Malayeri, M. R., & Riazi, M. (2018). Precipitation and deposition of Asphaltene in porous media: Impact of various connate water types. *Journal of Molecular Liquids*, 258, 124–132. https://doi.org/10.1016/j.molliq.2018.02.124
- Emmanuel, S., Ague, J. J., & Walderhaug, O. (2010). Interfacial energy effects and the evolution of pore size distributions during quartz precipitation in sandstone. *Geochimica et Cosmochimica Acta*, 74(12), 3539–3552. https://doi.org/10.1016/j.gca.2010.03.019
- Espinosa-Marzal, R. M., & Scherer, G. W. (2010). Advances in understanding damage by salt crystallization. *Accounts of Chemical Research*, 43(6), 897–905. https://doi.org/10.1021/ar9002224
- Falcon-Suarez, I. H., Livo, K., Callow, B., Marin-Moreno, H., Prasad, M., & Best, A. I. (2020). Geophysical early warning of salt precipitation during geological carbon sequestration. *Scientific Reports*, 10(1), 1–14. https://doi.org/10.1038/s41598-020-73091-3
- Fornea, A. P., Brooks, S. D., Dooley, J. B., & Saha, A. (2009). Heterogeneous freezing of ice on atmospheric aerosols containing ash, soot, and soil. *Journal of Geophysical Research*, 114(13), 1–12. https://doi.org/10.1029/2009JD011958
- Gao, Y., Xie, X., Wang, S., Tang, L., Geng, Z., & Li, J. (2022). Pore-scale experimental investigation of the remaining oil formation in water-wet, mixed-wet and oil-wet sandstone samples. *Journal of Petroleum Science and Engineering*, 216(December 2021), 110790. https://doi.org/10.1016/j.petrol.2022.110790
- Ge, B. B., Zhong, D. L., & Lu, Y. Y. (2019). Influence of water saturation and particle size on methane hydrate formation and dissociation in a fixed bed of silica sand. *Energy Procedia*, 158, 5402–5407. https://doi.org/10.1016/j.egypro.2019.01.623
- Godinho, J. R. A., Gerke, K. M., Stack, A. G., & Lee, P. D. (2016). The dynamic nature of crystal growth in pores. *Scientific Reports*, 6(August), 1–7. https://doi.org/10.1038/srep33086
- Gu, Y., Liu, X., Li, Y., Lu, H., Xu, C., Ren, J., et al. (2025). Feasibility analysis of liquid CO₂ injection and sequestration as hydrates in South China Sea marine sediments over 100 years. Applied Energy, 380(December 2024), 125068. https://doi.org/10.1016/j.apenergy.2024.125068
 Guida, B. S., Bose, M., & Garcia-Pichel, F. (2017). Carbon fixation from mineral carbonates. Nature Communications, 8(1), 1–6. https://doi.org/10.1038/s41467-017-00703-4
- He, D., Jiang, P., & Xu, R. (2019). Pore-Scale experimental investigation of the effect of supercritical CO₂ injection rate and surface wettability on salt precipitation. Environmental Science and Technology, 53(24), 14744–14751. https://doi.org/10.1021/acs.est.9b03323
- Helland, J. O., & Jettestuen, E. (2016). Mechanisms for trapping and mobilization of residual fluids during capillary-dominated three-phase flow in porous rock. Water Resources Research, 52(7), 5376–5392. https://doi.org/10.1002/2016WR018912
- Ji, T., Jiang, P., Chalaturnyk, R., Xu, R., Haghi, A. H., Jiang, P., et al. (2025). Capillary-Driven transport and precipitation of salt in heterogeneous structures during carbon sequestration. Geophysical Research Letters, 52(13), e2024GL114388. https://doi.org/10.1029/2024GL114388
- Lebeau, M., & Konrad, J. M. (2010). A new capillary and thin film flow model for predicting the hydraulic conductivity of unsaturated porous media. Water Resources Research, 46(1), 1–15. https://doi.org/10.1029/2010WR009092

LIU ET AL. 8 of 10



- 10.1029/2025GL118361
- Li, J., Zhang, Y., Di, S., Lin, L., & Zhou, Y. (2023). Research on hydrate-bearing reservoir deformation and wellbore wall stability during natural gas hydrate exploitation. Geomechanics for Energy and the Environment, 34, 100458. https://doi.org/10.1016/j.gete.2023. 100458
- Li, Q., Wang, Z., Guo, H., Zhao, J., Luo, H., & Huang, X. (2024). A perspective view of salt crystallization from solution in porous media: Morphology, mechanism, and salt efflorescence. Scientific Reports, 14(1), 23510. https://doi.org/10.1038/s41598-024-74645-5
- Liu, L., Zhang, Z., Li, C., Ning, F., Liu, C., Wu, N., & Cai, J. (2020). Hydrate growth in Quartzitic sands and implication of pore fractal characteristics to hydraulic, mechanical, and electrical properties of hydrate-bearing sediments. *Journal of Natural Gas Science and Engi*neering, 75(October 2019), 103109. https://doi.org/10.1016/j.jngse.2019.103109
- Liu, Q. (2025). Experimental and measurement data on crystal growth in a microfluidic chip [Dataset]. Zenodo. https://doi.org/10.5281/zenodo. 16406676
- Liu, Q., Li, S., Jiang, L., Yang, M., Yu, T., & Song, Y. (2025). Behaviors of methane hydrate formation and growth with halo. *Applied Energy*, 381(December 2024), 125131. https://doi.org/10.1016/j.apenergy.2024.125131
- Ma, J. F., Wang, X. L., Yang, A. Y., & Zhao, T. P. (2023). Tracking crystal-melt segregation and accumulation in the intermediate magma reservoir. Geophysical Research Letters, 50(10), e2022GL102540. https://doi.org/10.1029/2022GL102540
- Mehmani, Y., & Xu, K. (2022a). Advances in water resources capillary equilibration of trapped ganglia in porous media: A pore-network. Modeling approach. Advances in Water Resource, 166(May), 104223. https://doi.org/10.1016/j.advwatres.2022.104223
- Mehmani, Y., & Xu, K. (2022b). Pore-network modeling of Ostwald ripening in porous media: How do trapped bubbles Equilibrate. *Journal of Computational Physics*, 457, 17–20. https://doi.org/10.1016/j.jcp.2022.111041
- Moebius, F., & Or, D. (2014). Pore scale dynamics underlying the motion of drainage fronts in porous media. Water Resources Research, 50(11), 8441–8457. https://doi.org/10.1002/2014WR015916
- Mullin, J. W. (2001). Crystallization. Elsevier.
- Nooraiepour, M., Fazeli, H., Miri, R., & Hellevang, H. (2018). Effect of CO₂ phase States and flow rate on salt precipitation in shale Caprocks—A microfluidic study. *Environmental Science and Technology*, 52(10), 6050–6060. https://doi.org/10.1021/acs.est.8b00251
- Ou, W., Lu, W., Qu, K., Geng, L., & Chou, I. M. (2016). In situ Raman spectroscopic investigation of flux-controlled crystal growth under high pressure: A case study of carbon dioxide hydrate growth in aqueous solution. *International Journal of Heat and Mass Transfer*, 101, 834–843. https://doi.org/10.1016/j.ijheatmasstransfer.2016.05.082
- Pecher, I. A., Cook, A. E., Solomon, E. A., Wang, X., Han, S., Paganoni, M., et al. (2025). Dissociating gas hydrate beneath the hydrate stability zone. *Geophysical Research Letters*, 52(13), e2024GL112200. https://doi.org/10.1029/2024GL112200
- Poonoosamy, J., Obaied, A., Deissmann, G., Prasianakis, N. I., Kindelmann, M., Wollenhaupt, B., et al. (2023). Microfluidic investigation of pore-size dependency of barite nucleation. *Communications Chemistry*, 6(1), 1–12. https://doi.org/10.1038/s42004-023-01049-3
- Righter, K., & Downs, R. T. (2001). The crystal structures of synthetic Re- and PGE-bearing magnesioferrite spinels: Implications for impacts, accretion and the mantle. Geophysical Research Letters, 28(4), 619–622. https://doi.org/10.1029/2000GL012184
- Scherer, G. W. (2000). Stress from crystallization of salt in pores. In *Proceedings of the 9th International Congress on Deterioration and Conservation of Stone* (pp. 187–194). Elsevier Science B.V. Fassina (Ed.). https://doi.org/10.1016/B978-044450517-0/50100-8
- Schultz, R., Woo, J. U., Pepin, K., Ellsworth, W. L., Zebkar, H., Segall, P., et al. (2023). Disposal from in situ bitumen recovery induced the ML 5.6 Peace River earthquake. *Geophysical Research Letters*, 50(6), 1–10. https://doi.org/10.1029/2023GL102940
- Seyyedi, M., Mahmud, H. K. B., Verrall, M., Giwelli, A., Esteban, L., Ghasemiziarani, M., & Clennell, B. (2020). Pore structure changes occur during CO₂ injection into Carbonate reservoirs. Scientific Reports, 10(1), 1–14. https://doi.org/10.1038/s41598-020-60247-4
- Shaw, R. A., Durant, A. J., & Mi, Y. (2005). Heterogeneous surface crystallization observed in undercooled water. *The Journal of Physical Chemistry B*, 109(20), 9865–9868. https://doi.org/10.1021/jp0506336
- Shokri-Kuehni, S. M. S., Vetter, T., Webb, C., & Shokri, N. (2017). New insights into saline water evaporation from porous media: Complex interaction between evaporation rates, precipitation, and surface temperature. Geophysical Research Letters, 44(11), 5504–5510. https://doi.org/10.1002/2017GL073337
- Sloan, E. D. (1998). Clathrates hydrates of the natural gases. Marcel Dekker, New York. Retrieved from http://www.crcpress.com
- Sloan, E. D. (2003). Fundamental principles and applications of natural gas hydrates. Nature, 426(6964), 353–359. https://doi.org/10.1038/nature02135
- Sokama-Neuyam, Y. A., Yusof, M. A. M., Owusu, S. K., Darkwah-Owusu, V., Turkson, J. N., Otchere, A. S., & Ursin, J. R. (2023). Experimental and theoretical investigation of the mechanisms of drying during CO₂ injection into saline reservoirs. *Scientific Reports*, 13(1), 1–11. https://doi.org/10.1038/s41598-023-36419-3
- Stocker, R., & Hosoi, A. E. (2004). Corner flow in free liquid films. *Journal of Engineering Mathematics*, 50(2–3), 267–288. https://doi.org/10.1007/s10665-004-1243-1
- Sun, G., & Tanaka, H. (2024). Surface-induced water crystallisation driven by precursors formed in negative pressure regions. Nature Communications, 15(1), 4–6. https://doi.org/10.1038/s41467-024-50188-1
- Svoboda, J., Zickler, G. A., Kozeschnik, E., & Fischer, F. D. (2022). Generalization of classical Hillert's grain growth and LSW theories to a wide family of kinetic evolution equations and stationary distribution functions. *Acta Materialia*, 235, 118085. https://doi.org/10.1016/j.actamat. 2022.118085
- Titze, T., Lauerer, A., Heinke, L., Chmelik, C., Zimmermann, N. E. R., Keil, F. J., et al. (2015). Transport in nanoporous materials including MOFs: The applicability of Fick's laws. *Angewandte Chemie—International Edition*, 54(48), 14580–14583. https://doi.org/10.1002/anie. 201506954
- Tokunaga, T. K. (2009). Hydraulic properties of adsorbed water films in unsaturated porous media. Water Resources Research, 45(6), 1–9. https://doi.org/10.1029/2009WR007734
- Wu, R., Zhang, T., Ye, C., Zhao, C. Y., Tsotsas, E., & Kharaghani, A. (2020). Pore network model of evaporation in porous media with continuous and discontinuous corner films. *Physical Review Fluids*, 5(1), 1–21. https://doi.org/10.1103/PhysRevFluids.5.014307
- Wu, Z., Huang, Y., Chen, X., & Zhang, X. (2018). Capillary-driven flows along curved interior corners. *International Journal of Multiphase Flow*, 109, 14–25. https://doi.org/10.1016/j.ijmultiphaseflow.2018.04.004
- Xu, H., Liu, Y., He, S., Zheng, J., Jiang, L., & Song, Y. (2024). Enhanced CO₂ hydrate formation using hydrogen-rich stones, L-Methionine and SDS: Insights from kinetic and morphological studies. *Energy*, 291, 130280. https://doi.org/10.1016/j.energy.2024.130280
- Yan, L., Niftaliyev, R., Voskov, D., & Farajzadeh, R. (2025). Dynamics of salt precipitation at pore scale during CO₂ subsurface storage in saline aquifer. *Journal of Colloid and Interface Science*, 678(PB), 419–430. https://doi.org/10.1016/j.jcis.2024.08.265

LIU ET AL. 9 of 10



- 10.1029/2025GL118361
- Yang, Z., Niemi, A., Fagerlund, F., Illangasekare, T., & Detwiler, R. L. (2013). Dissolution of dense non-aqueous phase liquids in vertical fractures: Effect of finger residuals and dead-end pools. *Journal of Contaminant Hydrology*, 149, 88–99. https://doi.org/10.1016/j.jconhyd. 2013.03.006
- Zhang, J., Yin, Z., Khan, S. A., Li, S., Li, Q., Liu, X., & Linga, P. (2024). Path-dependent morphology of CH₄ hydrates and their dissociation studied with high-pressure microfluidics. *Lab on a Chip*, 24(6), 1602–1615. https://doi.org/10.1039/D3LC00950E
- Zhang, Z., Li, C., Ning, F., Liu, L., Cai, J., Liu, C., et al. (2020). Pore fractal characteristics of hydrate-bearing sands and implications to the saturated water permeability. *Journal of Geophysical Research: Solid Earth*, 125(3), 1–19. https://doi.org/10.1029/2019JB018721

LIU ET AL. 10 of 10